AGU PUBLICATIONS

JGR

Journal of Geophysical Research: Solid Earth

RESEARCH ARTICLE
10.1002/2017JB014325

Special Section:
Stress at Active Plate Boundaries - Measurement and Analysis, and Implications for Seismic Hazard

How fault evolution changes strain partitioning and fault slip rates in Southern California: Results from geodynamic modeling

Jiyang Ye[1,2] **and Mian Liu**[1]

[1]Department of Geological Sciences, University of Missouri, Columbia, Missouri, USA, [2]Now at Kalkulo AS, Simula Research Laboratory, Fornebu, Norway

Key Points:
- Numerical models show fault initiations and their impact on strain partitioning in Southern California over the past few million years
- New faults initiate to increase mechanical efficiency of accommodating the relative plate motion
- Slip rates between faults on the western and eastern sides of the San Andreas plate boundary zone are generally codependent

Supporting Information:
- Supporting Information S1

Correspondence to:
J. Ye,
ye@simula.no

Citation:
Ye, J., and M. Liu (2017), How fault evolution changes strain partitioning and fault slip rates in Southern California: Results from geodynamic modeling, *J. Geophys. Res. Solid Earth*, *122*, doi:10.1002/2017JB014325.

Received 12 APR 2017
Accepted 4 AUG 2017
Accepted article online 7 AUG 2017

Abstract In Southern California, the Pacific-North America relative plate motion is accommodated by the complex southern San Andreas Fault system that includes many young faults (<2 Ma). The initiation of these young faults and their impact on strain partitioning and fault slip rates are important for understanding the evolution of this plate boundary zone and assessing earthquake hazard in Southern California. Using a three-dimensional viscoelastoplastic finite element model, we have investigated how this plate boundary fault system has evolved to accommodate the relative plate motion in Southern California. Our results show that when the plate boundary faults are not optimally configured to accommodate the relative plate motion, strain is localized in places where new faults would initiate to improve the mechanical efficiency of the fault system. In particular, the Eastern California Shear Zone, the San Jacinto Fault, the Elsinore Fault, and the offshore dextral faults all developed in places of highly localized strain. These younger faults compensate for the reduced fault slip on the San Andreas Fault proper because of the Big Bend, a major restraining bend. The evolution of the fault system changes the apportionment of fault slip rates over time, which may explain some of the slip rate discrepancy between geological and geodetic measurements in Southern California. For the present fault configuration, our model predicts localized strain in western Transverse Ranges and along the dextral faults across the Mojave Desert, where numerous damaging earthquakes occurred in recent years.

1. Introduction

In Southern California, the ~49 mm/yr relative plate motion between the Pacific and North American plates [*DeMets et al*., 1994] has been distributed between the San Andreas Fault (SAF) and a complex system of young faults that together form a broad plate boundary zone (Figure 1). Hence, seismicity in Southern California is broadly distributed. Numerous damaging earthquakes in recent years, including the 1992 Landers earthquake (M_w 7.3), the 1999 Hector Mine earthquake (M_w 7.1), and the 1994 Northridge earthquake (M_w 6.7), occurred not on the SAF proper but on these diffuse young faults (Figure 1).

Most of these secondary faults in Southern California initiated in the past 2 Ma (Table 1), likely a necessity to compensate for the reduced slip by irregularities of the SAF proper. The Big Bend, a major restraining bend of the SAF related to the opening of the Gulf of California between 12 and 5 Ma [*Stock and Hodges*, 1989; *Holt et al*., 2000; *Oskin and Stock*, 2003], impedes slip on the SAF and causes diffuse shear stresses in much of Southern California [*Li and Liu*, 2006]. It may have played a major role in the initiation of the Eastern California Shear Zone [*Liu et al*., 2010]. Likewise, the San Bernardino restraining bend may have caused strain localization and contributed to the activation of the San Jacinto Fault in the past 2 Ma [*Li and Liu*, 2007]. *Cooke and Dair* [2011] used a three-dimensional boundary element model to show that the southern Big Bend of the SAF has evolved to its present configuration in the past one million years by abandoning two active fault strands, to increase its mechanical efficiency in accommodating the relative plate motion.

The fault evolution in Southern California implies continuous changes of strain partitioning across the plate boundary zone and slip rates on all faults in the system. The present-day slip rates on many of these faults in Southern California have been well constrained by space geodetic measurements; exceptions are the blind faults in western Transverse Ranges, the diffuse faults across the Mojave Desert, and the offshore faults where GPS measurements are sparse [*Becker et al*., 2005; *McCaffrey*, 2005; *Meade and Hager*, 2005; *Spinler et al*., 2010; *Loveless and Meade*, 2011; *Johnson*, 2013; *McGill et al*., 2015; *Zeng and Shen*, 2016]. However, the slip rates

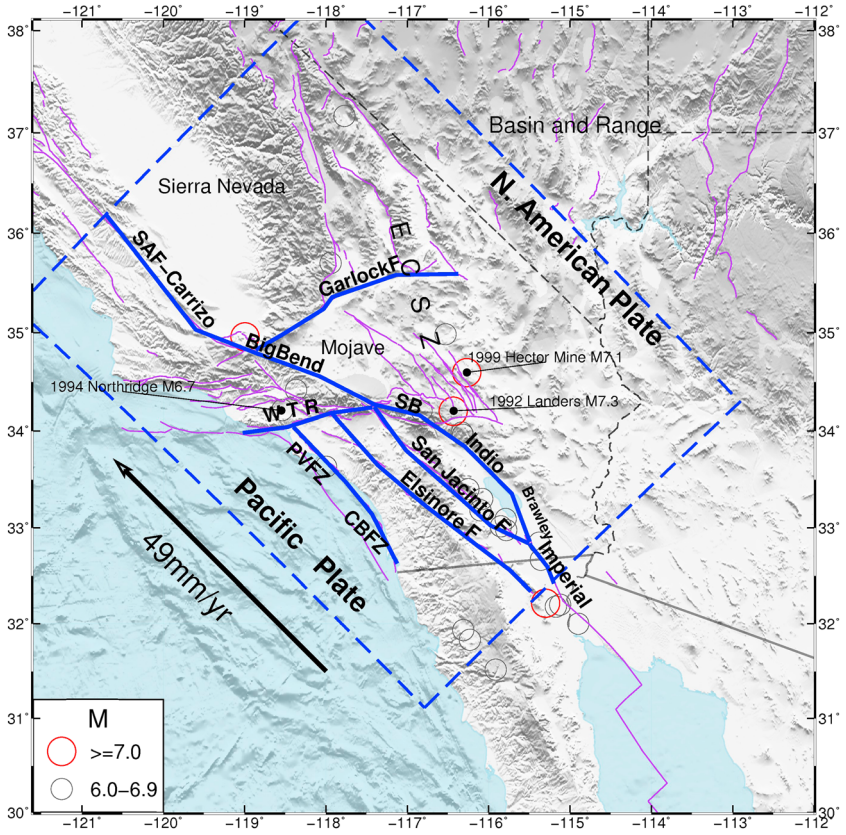

Figure 1. Topographic relief, active faults, and seismicity in the Southern California plate boundary zone. SAF: the San Andreas Fault; SB: San Bernardino segment; PVFZ: Palos Verdes Fault zone; CBFZ: Coronado Bank Fault zone; WTR: western Transverse Ranges; ECSZ: the Eastern California Shear Zone. Thin purple lines represent the active faults, thick blue lines are the faults implemented in the finite element model, and blue dashed lines are the model boundary. Circles are epicenters of seismic events ($M > 6$).

constrained from geodetic data differ from geological estimates on many faults [*Oskin et al.*, 2008; *Bird*, 2009; *Chuang and Johnson*, 2011; *Loveless and Meade*, 2011; *Lindsey and Fialko*, 2013; *Tong et al.*, 2014; *Zeng and Shen*, 2014; *McGill et al.*, 2015; *Evans et al.*, 2016]. The discrepancies may arise from the uncertainty of geodetic inversion methods [*Johnson*, 2013], or geological measurements [*Bird*, 2007; *Zechar and Kurt*, 2009], or both; but some of the discrepancies are likely due to the different timescales of the geodetic and geological data, the latter reflect longer timescales during which the fault slip rates may have changed by the initiation of new faults in the plate boundary zone [*Morton and Matti*, 1993; *Bennett et al.*, 2004].

Table 1. Estimated Timing of Fault Initiation in the Southern California Plate Boundary Zone

Fault Name	Initiation Time	References
Southern SAF	5–8 Ma	*Atwater* [1970] and *Atwater and Stock* [1998]
Garlock Fault	5–8 Ma	*Stock and Hodges* [1989], *Holt et al.* [2000], and *Oskin and Stock* [2003]
San Jacinto Fault	1.1–2.5 Ma	*Morton and Matti* [1993], *Lutz et al.* [2006], and *Janecke et al.* [2011]
N. Elsinore Fault	~2.5 Ma	*Hull and Nicholson* [1992] and *Magistrale and Rockwell* [1996]
S. Elsinore Fault	~1.2 Ma	*Dorsey et al.* [2012]
Palos Verdes– Coronado Bank Fault zone	≤1 Ma 2.4–3 Ma	*Dolan et al.* [1995] and *McNeilan et al.* [1996] *Ward and Valensise* [1994]
Thrust faults in	2–3 Ma	*Namson and Davis* [1988]
Western transverse ranges	~0.5 Ma	*Huftile and Yeats* [1995]
ECSZ- Mojave fault	≤0.85 Ma	*Oskin et al.* [2008]

In this study, we use the three-dimensional viscoelastoplastic finite element model [*Li and Liu*, 2006; *Li et al*., 2009; *Liu et al*., 2010] to systematically investigate the evolution of the SAF plate boundary zone in Southern California in the past few million years. We do not intend to answer the question of how the young faults in Southern California developed, because fault development is controlled by both stress and strain localization due to tectonics forces and the inherited lithospheric heterogeneities; the latter is poorly constrained and difficult to implement in numerical models. Instead, given the geologically recorded developments of these young faults, we investigate here how the initiation of these young faults may have changed strain partitioning and slip rate of major faults in Southern California.

2. The Southern California San Andreas Fault System

The San Andreas Fault is a transform plate boundary between the Pacific and the North American plates [*Atwater*, 1970; *Wallace*, 1990], with a total of ~49 mm/yr relative plate motion [*DeMets et al*., 1994; *Bennett et al*., 1996]. In Southern California, the plate boundary comprises the southern SAF (SSAF) proper, a system of subparallel dextral strike-slip faults to its west, numerous dextral faults across the Mojave Desert that form the southern section of the Eastern California Shear Zone (ECSZ), the east-west trending sinistral Garlock Fault, and the thrust faults in the western Transverse Ranges (Figure 1). The SSAF proper accommodates about 50–75% of the present-day relative plate motion [*Becker et al*., 2005; *McCaffrey*, 2005; *Meade and Hager*, 2005]; the rest are taken up by slip on the ECSZ [*Dokka and Travis*, 1990; *Gan et al*., 2000; *Peltzer et al*., 2001; *Dixon et al*., 2003], the San Jacinto Fault [*Sharp*, 1981; *Rockwell et al*., 1990; *Morton and Matti*, 1993; *Bennett et al*., 2004; *Becker et al*., 2005], and the other faults.

The SAF originated around 29 Ma when the subduction of the Farallon plate brought the encounter of the Pacific plate with the North American plate [*Atwater*, 1970; *Atwater and Stock*, 1998]. The current configuration of the SAF proper largely developed by ~5 Ma, when the opening of the Gulf of California and rotation of the borderland blocks caused the SAF to jump inland and form the Big Bend, a major restraining bend of the SAF (Figure 1) [*Atwater and Stock*, 1998; *Oskin and Stock*, 2003].

The Garlock Fault and the ECSZ both initiated around the same time as the opening of the Gulf of California [*Stock and Hodges*, 1989; *Holt et al*., 2000; *Oskin and Stock*, 2003]. The Garlock Fault was perhaps related to the Basin and Range extension [*Davis and Burchfiel*, 1973]. Development of the ECSZ has also been related with a kinematic change around ~8 Ma when the Sierra Nevada-Great Valley block switched from moving westerly, driven by the Basin and Range extension, to its modern NW directed motion [*Wernicke and Snow*, 1998], as witnessed by a change in stress direction in the Walker Lane belt (also referred to as the northern section of the ECSZ) about 7–10 Ma [*Zoback et al*., 1981; *Bellier and Zoback*, 1995]. South of the Garlock Fault, the ECSZ consists of a system of NW trending dextral faults cutting across the Mojave Desert [*Dokka and Travis*, 1990] (Figure 1). Some of these faults are less than one million years old. The total slip rate on the ECSZ across the Mojave Desert is about 6 mm/yr estimated by geological measurements [*Kirby et al*., 2006; *Oskin et al*., 2008] and up to 12 mm/yr based on geodetic inversion [*Becker et al*., 2005; *Loveless and Meade*, 2011].

To the southwest side of the SAF proper are the subparallel San Jacinto Fault and other secondary NW trending dextral faults, including the Elsinore Fault and numerous offshore faults (the Palos Verdes Fault Zone and the Coronado Bank Fault Zone). The initial offset time and the geological slip rate on the San Jacinto Fault are still controversial; estimates ranging from 1.1–1.4 Ma [*Lutz et al*., 2006; *Janecke et al*., 2011] to 1.8–2.5 Ma [*Morton and Matti*, 1993] for its age and around 12 mm/yr [*Rockwell et al*., 1990; *Blisniuk et al*., 2013] to 20 mm/yr [*Morton and Matti*, 1993; *Janecke et al*., 2011] for the geological slip rate. The present-day slip rate on the SJF is ~15 ± 9 mm/yr [*Becker et al*., 2005] or higher [*Lundgren et al*., 2009].

The age of the subparallel dextral faults further to the west are generally younger. The initiation of the southern Elsinore Fault was about 1.2 Ma, and the lifetime slip rate is around 1–2 mm/yr [*Dorsey et al*., 2012]. The northern section of the Elsinore fault may have initiated earlier, around 2.5 Ma, with lifetime slip rate around 3–6 mm/yr [*Hull and Nicholson*, 1992; *Magistrale and Rockwell*, 1996]. The age for the Palos Verdes Fault Zone and other offshore faults are poorly constrained partly because of the offshore location and the complex fault structure. They are generally around or less than 1 Ma (Table 1). The slip rate on the Palos Verdes Fault Zone was ~3 mm/yr for the past 8 ka [*Dolan et al*., 1995; *McNeilan et al*., 1996]; the Coronado Bank Fault Zone has a slip rate $\leq$ 1 mm/yr during the Holocene [*Hill*, 1971; *Grant et al*., 1997; *Grant and Shearer*, 2004].

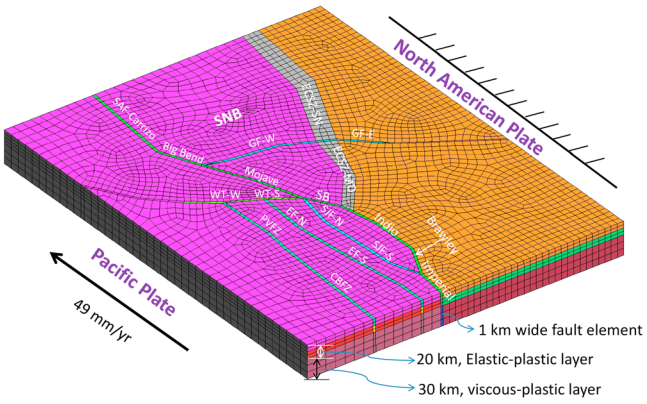

Figure 2. Numerical mesh and boundary conditions of the finite element model. The model consists of an elastoplastic upper crust (20 km) and a viscoelastic lower crust and mantle (30 km). The faults are represented by a thin (1 km) layer of fault elements with low plastic strength. The southern San Andreas Fault is divided into seven segments: the Carrizo segment (SAF-Carrizo), the Big Bend, Mojave segment, San Bernardino segment (SB), Indo segment, Brawley segment, and the Imperial fault. GF-W and GF-E: western and eastern segments of the Garlock Fault; SJF-N and SJF-S: northern and southern segments of the San Jacinto Fault; EF-N and EF-S: northern and southern segments of the Elsinore Fault; PVFZ: the Palos Verdes Fault zone; CBFZ: the Coronado Bank Fault zone; WT-W and WT-E: western and eastern thrust faults in western Transverse Ranges; ECSZ-SN and ECSZ-MD: the Eastern California Shear Zone in Sierra Nevada and Mojave Desert; SNB: the Sierra Nevada Block.

3. FEM Model

To investigate the mechanics of long-term fault evolution and interaction in Southern California, we use a three-dimensional viscoelastoplastic finite element method developed by *Li et al.* [2009]. An important feature of this code is the inclusion of plastic strain: it uses steady state plastic creep on the fault zones to simulate long-term fault slip, and it allows plastic strain to occur in the crust outside the fault zones when the plastic yield is reached. In places of highly localized plastic strain, initiation of new faults (or reactivation of pre-existing faults) may be expected [*Li and Liu*, 2007; *Li et al.*, 2009; *Liu et al.*, 2010; *Ye et al.*, 2015]. Detailed description of this code is given by *Li et al.* [2009]; here we briefly describe the model setup for this study (Figure 2).

To simulate the long-term behavior of fault evolution, we assume that the lithospheric deformation follows the continuum mechanics. The model calculates long-term, quasi-static deformation of the three-dimensional lithosphere, which follows the equation of force equilibrium [*Cook et al.*, 2002; *Li et al.*, 2009]:

$$\frac{\partial \sigma_{ij}}{\partial x_j} + f_i = 0 \tag{1}$$

where $\sigma_{ij}(i,j = x,y,z)$ are components of the stress tensor, f_i are components of the body force vector. For the Southern California transform plate boundary zone, we assume that the deviatoric stresses arise mainly from the relative motion between the Pacific and North American plates. The model boundary conditions are described in the following (Figure 2). The northern and southern sides of the model domain are traction free. The top surface of the model is also traction free, while the bottom is fixed in the vertical direction and traction free in the horizontal direction. The eastern side of the model domain is fixed, simulating the stable North American plate. The western side is loaded by shearing at 49 mm/yr, reflecting the relative plate motion in Southern California [*DeMets et al.*, 1994].

The model domain consists of an elastoplastic upper crust and a viscoelastic lower crust and mantle (Figure 2). The faults are represented by thin (1 km) layers of fault elements with a lower plastic-yielding strength than that of the surrounding crust. Under the imposed loading, the fault zones creep plastically when stress reaches the Drucker-Prager plasticity criterion [*Drucker and Prager*, 1952; *Li et al.*, 2009]. Similarly, plastic strain occurs and accumulates outside the fault zones where the stress reaches the plastic yield. The yield function for the Drucker-Prager model is

$$F = \alpha I_1 + \sqrt{J_2'} - k \tag{2}$$

where I_1 and J_2' are the first invariant of the stress tensor and the second invariant of the deviatoric stress tensor, respectively; the parameters α and k are related to the coefficient of friction and cohesion, respectively.

Table 2. Major Model Parameters in the Model

Material Block	Viscosity (Pa s)	Frictional Coefficient	Cohesion (MPa)
Upper crust	10^{25}	0.4	50
Lower crust and mantle	10^{21}	0.4	50
Fault within the upper crust	10^{25}	0–0.1	10 (SAF) 30 (other faults)
Fault downward extension	10^{21}	0–0.1	10 (SAF) 30 (other faults)

The plastic yield strength (in terms of α and k) assigned to the fault zones are lower than that for the crust (Table 2). For the viscoelastic lower layer, we used the viscosity of 10^{21} Pa s in most cases. The elastic constants for the entire model domain are conventional values for the lithosphere: 8.75×10^{10} Pa for the Young's modulus and 0.25 for the Poisson's ratio [*Li et al*., 2009; *Liu et al*., 2010].

4. Model Results

To explore how the southern SAF system may have evolved following the formation of the Big Bend, and how each new fault affects the regional strain partitioning and fault slip rates in Southern California, we conducted a series of forward models. We started with a simple case with only the SAF proper included in the model. This case serves as a reference model to demonstrate how the irregularities of fault geometry, in this case the Big Bend, affect slip rates along the SAF and strain partitioning in Southern California. We then incorporated the major secondary young faults in Southern California individually, based on their estimated chronological orders of initiation, into the model to investigate how the addition of each new fault changes the slip rates on all faults in the system and alters regional strain partitioning.

4.1. How Fault Geometry Impacts Strain Partitioning and Slip Rates

Figure 3 shows the results of the reference case, when the SAF proper is the only fault included in the model. If the SAF is a perfect transform plate boundary—straight and parallel to the direction of the relative plate motion, the model would predict perfect block motion, with every part of the Pacific plate moving coherently as a block relative to the fixed North American plate [*Liu et al*., 2010]. However, the Big Bend of the SAF, a restraining bend, impedes the motion of the Pacific plate. Because of the bend, the Pacific plate causes the edge of the North American plate (the Mojave Desert and the Sierra Nevada Block) to move with it (Figure 3a). This produces a broad zone of horizontal velocity gradients across the Big Bend between the two plates.

The relative plate motion not accommodated by steady state fault slip on the SAF needs to be compensated elsewhere, by plastic strain outside the fault (Figure 3b). The predicted plastic strain is highly localized in two belts, extending from the two ends of the Big Bend and subparallel to the direction of relative plate motion.

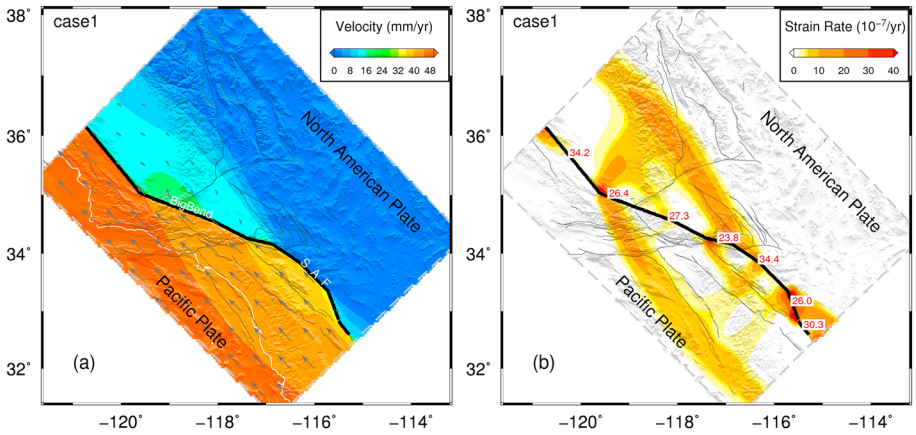

Figure 3. Results of the reference model that includes only the southern SAF proper (thick black line). (a) Surface horizontal velocity (arrows and color contours) relative to the fixed North America. White line is the coastline. (b) Plastic strain rate outside the SAF. Fault slip rates (in mm/yr) are average values for each modeled SAF segment.

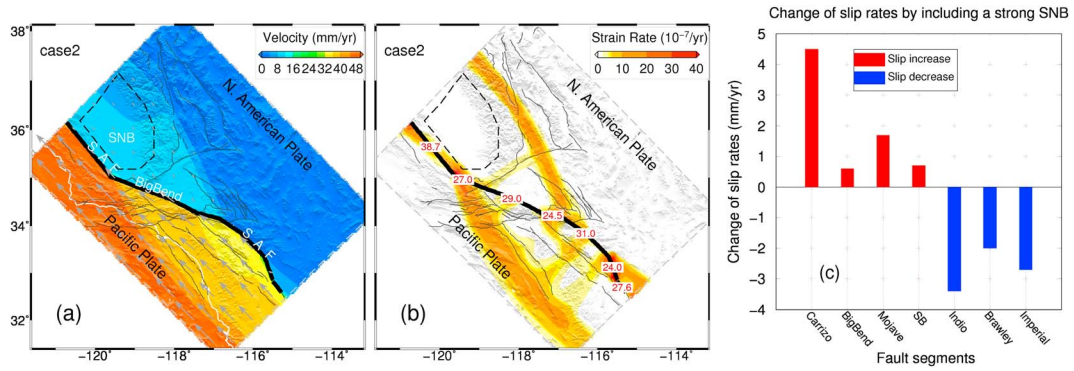

Figure 4. Effects of including a strong Sierra Nevada Block (SNB, outlined by the dashed lines). The SNB is given a high cohesion (60 MPa); other parameter values are given in Table 2. (a) Surface horizontal velocity relative to fixed North America. (b) Plastic strain rate outside the modeled fault segments (thick lines); fault slip rates (in mm/yr) are average values on each segment. (c) The change of fault slip rates relative to the reference case in Figure 3. The fault segments are defined in Figure 2.

One of the high-strain belts overlaps with the Eastern California Shear Zone, and the other overlaps with the offshore fault zones in Southern California.

Because the lithospheric rheology outside the fault zone is laterally homogeneous in this case, the predicted strain localization is entirely due to the stress variations induced by the fault irregularities and the plasticity. In the Drucker-Prager model of plasticity, the plastic yield depends on both the normal stress and shear stress (equation (2))—compressive normal stress hinders plastic yield, whereas shear stress promotes it. Around the Big Bend, the shear stress is high, but so is the compressive normal stress (Figure S1 in the supporting information), so the plastic strain is limited (Figure 3b). Along the two belts of localized strain, the shear stress is high (as can be inferred from the horizontal velocity gradients in Figure 3a), and the normal stress is relatively low. A model case with details of the accumulation of plastic strain around a restraining bend is provided in Figure S2.

The predicted fault slip rates as shown in Figure 3b depend on the plastic yield strength of the fault zone in the model. We adjusted the fault properties (cohesion and internal friction) such that the predicted slip rate on the Carrizo segment agrees with the geological slip rate of ~34 mm/yr (Appendix B of the UCERF 3, http://pubs.usgs.gov/of/2013/1165/). The fault properties are uniform in the model, so the reduced slip rates along the Big Bend result from its impedance to the relative plate motion.

4.2. Effects of Lithospheric Rheology

The predicted strain partitioning may vary with lithospheric rheology. Figure 4 shows the results when we increased the plastic strength of the Sierra Nevada Block (SNB) (Figure 4a), which is known to have behaved as a rigid block [*Dixon et al.*, 2000]. Having a strong SNB limits the plastic strain to a narrower zone along the ECSZ while increases the plastic strain along the offshore areas in Southern California (Figure 4b), which compensates for the reduced plastic strain on the eastern side of the SAF. Comparing with the reference model in Figure 3, including a strong SNB decreases slip rates on the southernmost segments of the SAF while it increases slip rates on the Carrizo segment, as well as along the coastal region (Figure 4c).

In the next case, we also lowered the plastic yield strength of the crust along the ECSZ, which are not explicitly included in the model as faults (Figure 5). Not surprisingly, this increases plastic strain rates along the ECSZ, at the expense of plastic strain along the coastal region. Similar results are found by *Liu et al.* [2010] by reducing the viscosity of the lower crust and upper mantle under the Basin and Range Province to the east of the ECSZ.

Consequently, the ECSZ is predicted to see an increase in slip rates (more precisely, shearing rates, as the ECSZ faults are not explicitly included in the model) (Figure 5c). A weak ECSZ also promotes slip on the southernmost segments of the SAF proper, perhaps by providing an easier path along the eastern side of the plate boundary zone to accommodate the relative plate motion (Figure 5b). This would relieve the burden on the Carrizo and Big Bend segments of the SAF proper, explaining the reduced slip there (Figure 5c).

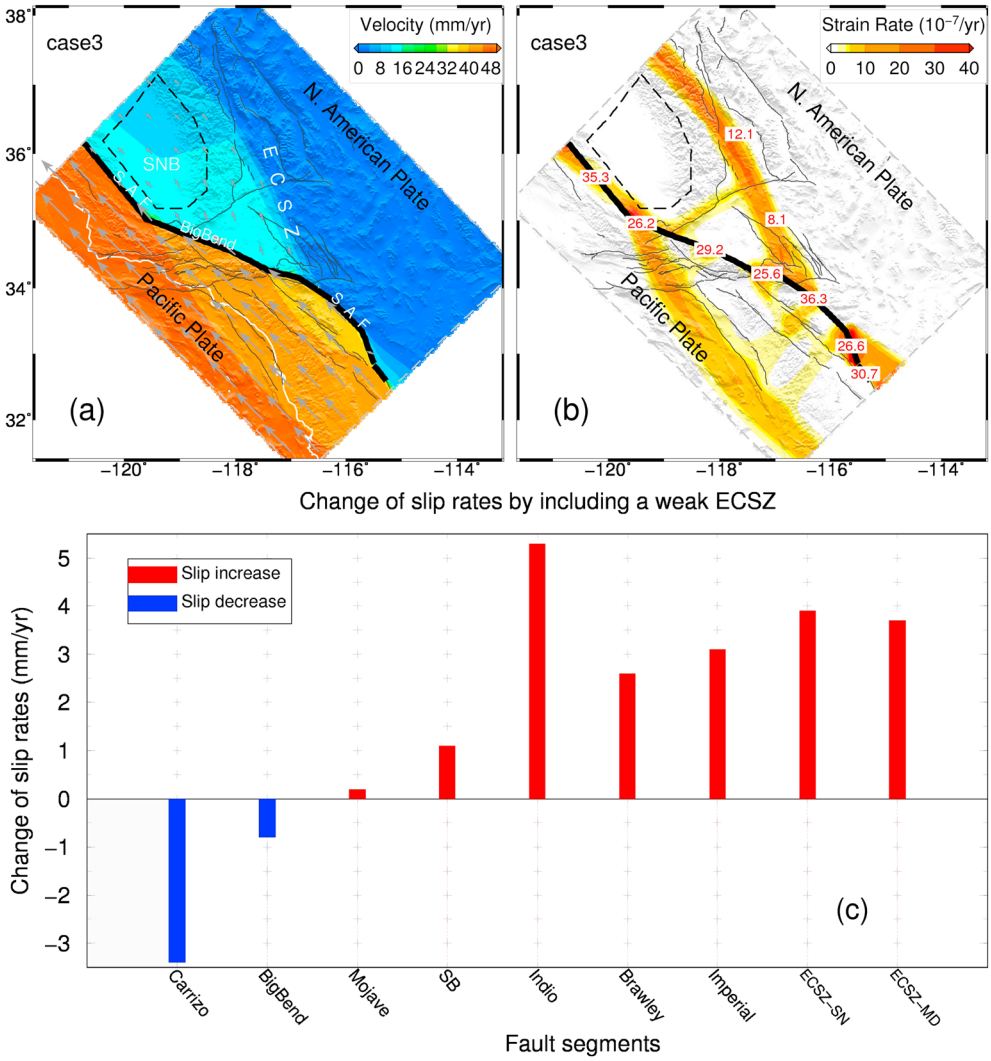

Figure 5. Effects of including a weak Easter California Shear Zone (ECSZ), simulated by reducing the cohesion of the crust to 40 MPa. Other parameter values are in Table 2. (a) Surface horizontal velocity. White line is the coastline. (b) Plastic strain rate outside the fault segments (thick lines); slip rates (in mm/yr) are average values for each fault segment. For ECSZ, where no faults are explicitly included in the model, slip rates are average values of the shearing rates across the fault zone. (c) The change of fault slip rates relative to the previous case in Figure 4. The fault segments are defined in Figure 2.

The rigid SNB and relatively weaker ECSZ crust are among the most noticeable rheological variations in Southern California; their effects on the SAF slip rates are less than 5 mm/yr (Figures 4c and 5c). The impact of other rheological heterogeneities not included in the model is likely less.

4.3. Effects of the Garlock Fault

The nearly 260 km long, roughly E-W striking Garlock Fault is an important boundary separating the Sierra Nevada Block and the Basin and Range province to the north from the Mojave Desert block to the south. It probably initiated around the same time as the formation of the Big Bend [*Burbank and Whistler*, 1987; *Monastero et al*., 1997], perhaps as a conjugate fault pair with the SAF to accommodate some of the convergence at the Big Bend section of the plate boundary fault [*Hill and Dibblee*, 1953; *McGill et al*., 2009]. Others have suggested that its formation is related to the Basin and Range extension [*Davis and Burchfiel*, 1973]. In the models that do not include the Garlock fault (Figures 3–5), a band of relatively high plastic strain is nonetheless predicted near the location of the Garlock Fault. This strain localization results from the Big Bend and the relatively stronger SNB, thus both may have contributed to the initiation of the Garlock Fault.

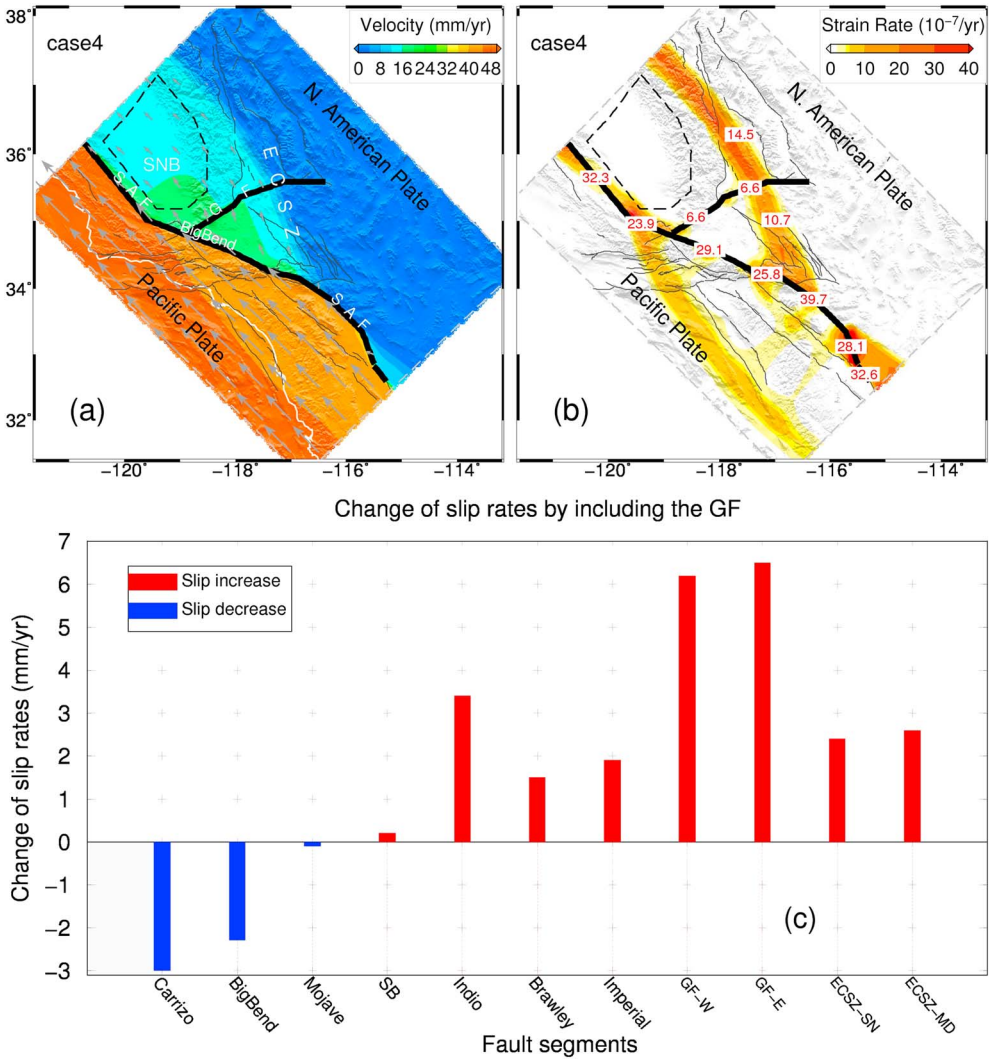

Figure 6. Effects of including the Garlock Fault (GF). (a) Surface horizontal velocity. White line is the coastline. (b) Plastic strain rate outside the faults (thick lines) and the fault slip rate (in mm/yr). (c) The change of fault slip rates relative to the previous case in Figure 5. The fault segments are defined in Figure 2.

Explicitly including the Garlock fault in the model does not significantly change the predicted surface velocity and strain localization (Figures 6a and 6b), but it has noticeable impact on the fault slip rates (Figure 6c). The biggest change, naturally, is the 6–7 mm/yr slip on the Garlock Fault, comparable with the geological estimates [*McGill et al.*, 2009; *Ganev et al.*, 2012]. However, the Garlock Fault also promotes slip on the ECSZ and the southernmost segments of the SAF, while it reduces slip rates on the Carrizo and the Big Bend segments. Essentially, the Garlock Fault further impedes relative motion along the Big Bend and the SAF segments farther north, thus forces more plastic strain to localize along the ECSZ, which in turn promotes slip on the southern segments of the SAF that are aligned with the ECSZ.

4.4. Effects of the San Jacinto Fault

The San Jacinto Fault formed around the same time as the restraining bend over the San Bernardino Mountains segment of the SAF, developed around 1.5–2 Ma [*Morton and Matti*, 1993; *Albright*, 1999; *Dorsey*, 2002]. This restraining bend may have localized strain and contributed to the development of the SJF [*Li and Liu*, 2007]. Explicitly adding the SJF in the model causes the horizontal velocity gradient to be largely limited to the zone between the SJF and the SAF (Figure 7a). Slip on the SJF reduces plastic strain along the coastal region (Figure 7b) and slip rates on the southernmost segments of the SAF (Figure 7c).

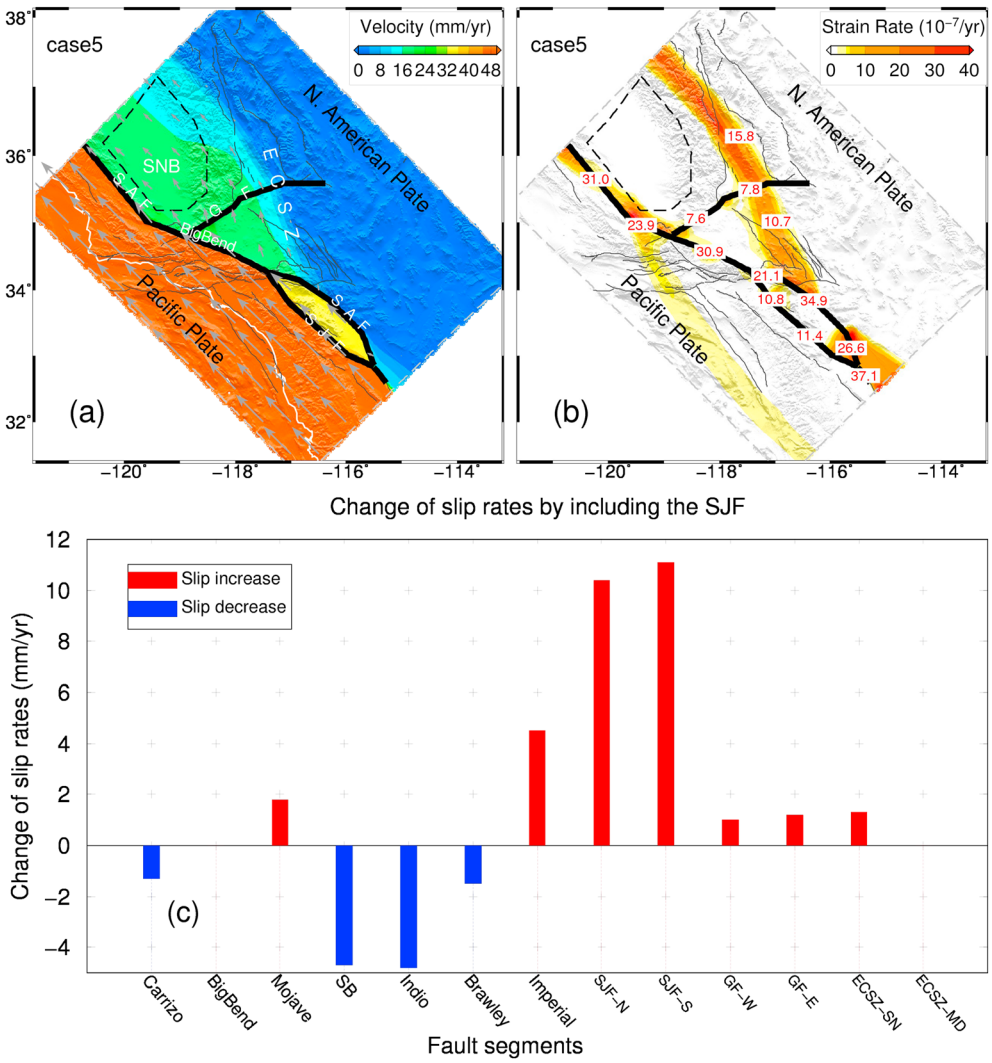

Figure 7. Effects of including the San Jacinto Fault (SJF). (a) Surface horizontal velocity. White line is the coastline. (b) Plastic strain rate outside the faults (thick lines) and the fault slip rate (in mm/yr). (c) The change of fault slip rates relative to the previous case in Figure 6. The fault segments are defined in Figure 2.

4.5. Effects of the Elsinore Fault and the Offshore Faults

The Elsinore Fault and the subparallel offshore faults, including the Palos Verdes Fault Zone and the Coronado Bank Fault Zone, are dextral NW trending strike slip faults initiated in the past one million years or so [*Hill*, 1971; *Dolan et al.*, 1995; *McNeilan et al.*, 1996; *Grant et al.*, 1997; *Grant and Shearer*, 2004]. The cause of these faults remains uncertain. It may also be related to the strain localization due to the Big Bend—as shown in previous figures (Figures 4–7), plastic strain is localized along the offshore region because of the impedance of the Big Bend to the relative plate motion. However, the Big Bend formed a few million years earlier, so additional factors must be involved to account for the recent initiation of these faults.

In the next case we added two faults in the model, one simulates the Elsinore Fault, the other simulates the offshore fault zones (Figure 8). The resulting surface velocity field shows a distributed relative motion across these faults (Figure 8a), as indicated by geodetic measurements [*Bourne et al.*, 1998; *Zeng and Shen*, 2016]. Slip on the Elsinore and the offshore faults tends to reduce the shear strain on the ECSZ needed to accommodate the relative plate motion. On the other hand, termination of the Elsinore and the offshore faults on their northern ends causes high plastic strain in the western Transverse Ranges (Figure 8b).

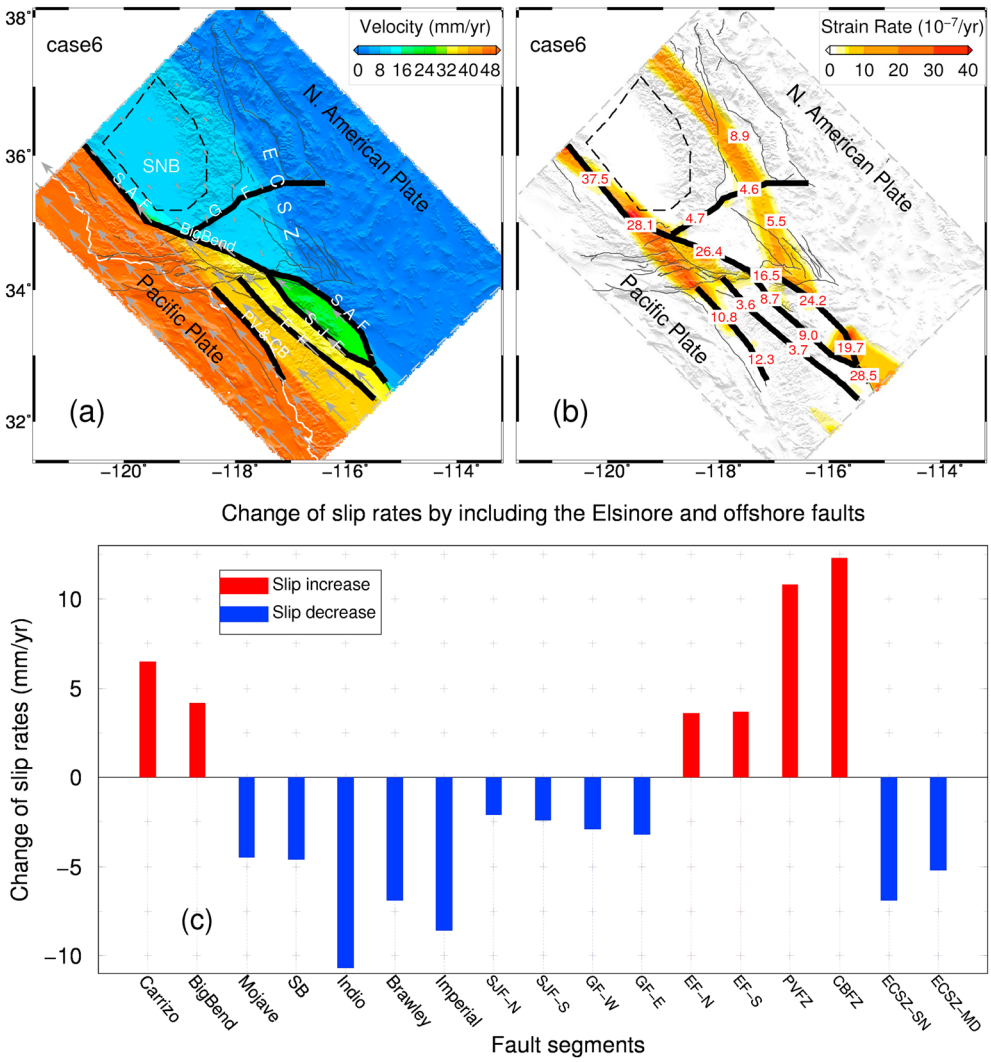

Figure 8. Effects of including the Elsinore Fault (EF) and the offshore dextral faults (Palos Verdes (PVFZ) and the Coronado Bank Fault zone (CBFZ)). (a) Surface horizontal velocity. White line is the coastline. (b) Plastic strain rate outside the faults (thick lines) and the fault slip rate (in mm/yr). (c) The change of fault slip rates relative to the previous case in Figure 7. The fault segments are defined in Figure 2.

The initiation of the Elsinore and the offshore faults made the western side of the plate boundary zone more efficient in accommodating the relative plate motion. Thus, slip rates reduce on the southernmost segments of the SAF, the San Jacinto Fault, and the ECSZ, while slip rates increase on the northern segments of the southern SAF (Figure 8c).

The predicted slip rates on the offshore faults are too high comparing with the geodetic rates and geological estimates, which are less than 3 mm/yr [*Dolan et al.*, 1995; *McNeilan et al.*, 1996; *Zeng and Shen*, 2016]. One explanation is that the impedance of the Big Bend has less impact on the offshore faults than on the SJF and southern SAF, and in the model we assumed the same fault strength for all secondary faults (Table 2). Young faults usually have higher strength than more mature faults [*Bird and Kong*, 1994]. If we assign higher strength to these young faults, the predicted slip rates would be lower and closer to the observed values, as shown in previous studies [*Li and Liu*, 2007].

4.6. The Thrust Faults in the Western Transverse Ranges

The thrust faults, including numerous blind faults, in the WTR pose serious seismic hazard to the Los Angeles metropolitan region [*Dolan et al.*, 1995], as illustrated by the 1994 Northridge earthquake (*Mw* 6.7). Figure 8b

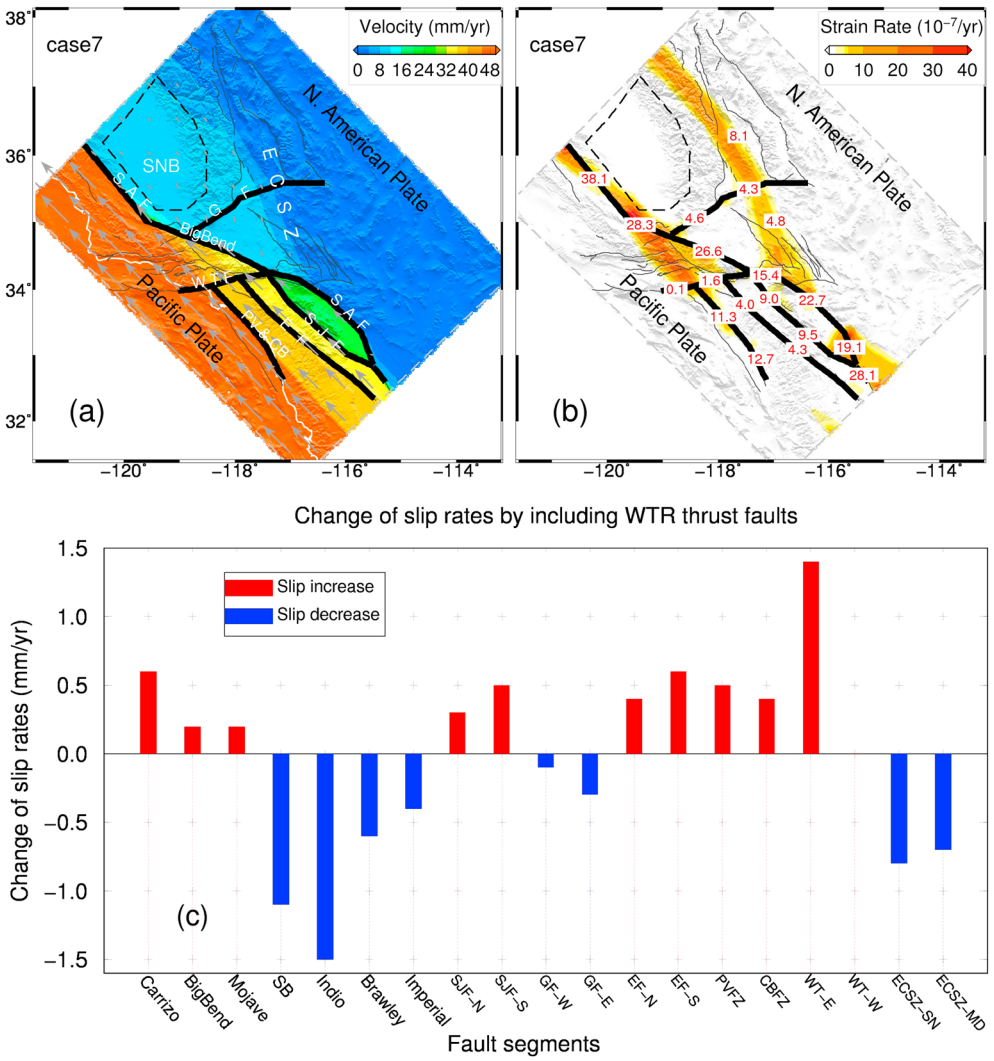

Figure 9. Effects of including the thrust faults in the western Transverse Ranges (WTR). (a) Surface horizontal velocity. White line is the coastline. (b) Plastic strain rate outside the faults (thick lines) and the fault slip rate (in mm/yr). (c) The change of fault slip rates relative to the previous case in Figure 8. The fault segments are defined in Figure 2.

shows that the initiation of the Elsinore and the offshore faults tends to localize strain in the WTR, which acts as a stepover interrupting the dextral crustal motion along the western side of the plate boundary zone. Such strain localization would have contributed to the activation of the thrust faults in the WTR and the associated seismicity.

In Figure 9 we show the results of explicitly adding a fault representing the thrust faults in the WTR. The resulting surface velocity field (Figure 9a) is similar to that in the previous case (Figure 8a). Having the roughly E-W trending fault zone in the WTR does not relieve much of the impedance to the dextral crustal motion across the WTR, so the high plastic strain here remains (Figure 9b). The WTR fault in the model is vertical for simplicity; a dipping thrust fault may be more accommodating for the crustal motion. Nonetheless, the results indicate that the WTR thrust faults promote slip on the dextral faults to the west of the SAF, including the northern segments of the southern SAF. Meanwhile, slip on the southernmost segments of the SAF fault, as well as the Garlock Fault and the ECSZ, is slightly reduced (Figure 9c).

This case includes all the major faults in Southern California, thus the results in Figure 9 represent the present strain partitioning and fault slip rates in the region. Of particular interest is the high strain rates predicted in western Transverse Ranges and the ECSZ across the Mojave Desert. Fault slip rates in these places are not well

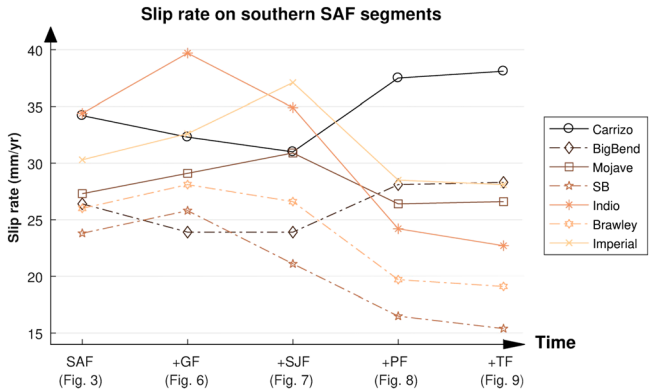

Figure 10. Predicted slip rate changes on each SAF segment (defined in Figure 2) with the initiation (inclusion in the model) of each additional fault (marked in the horizontal axis) in Southern California.

constrained by geodetic measurements because the faults are either blind or diffuse. Without explicitly including faults in these regions, our model nonetheless predicts high strain rates, which partially explains the numerous damaging earthquakes in these places.

The corresponding stress fields for the present fault configuration in Southern California are provided in the supporting information. The maximum shear stress and mean normal stress (Figure S3) are similar to previous models [*Li and Liu*, 2006], and the principal stresses are generally consistent with previous models [*Flesch et al*., 2000] and measurements [*Townend and Zoback*, 2004] (Figure S4).

5. Discussion

In our model the driving force is traction along the plate boundary due to relative plate motion. We did not include the gravitational potential energy that can be important for orogenic deformation [*England and Molnar*, 1997; *Flesch et al*., 2000], because our focus here is on fault slip within the San Andreas transform plate boundary. Our model does not exclude the effects of basal traction, which has been suggested by some workers as being important for the San Andreas plate boundary zone [*Bourne et al*., 1998]. However, basal traction is more difficult to constrain than relative plate motion.

For a given configuration of faults, our model predicts both the fault slip rates and distribution of plastic strain. The predicted strain localization outside faults provides some helpful insight into fault development, as detailed in our previous studies [*Li and Liu*, 2006, 2007; *Liu et al*., 2010]. In this study, we have focused on the impact of initiating new faults on the regional strain partitioning and fault slip rates. We have showed that in the past few million years, strain partitioning and fault slip rates in Southern California have continuously changed because of the initiation of new faults.

5.1. Fault Evolution and Variations of Fault Slip Rates

The fault configuration of the SAF plate boundary zone in Southern California has changed significantly in the past few million years. By ~5 Ma the opening of the Gulf of California caused the inland jump of the SAF, forming the restraining Big Bend. The Big Bend impedes the relative plate motion on the SAF, the main plate boundary fault, thus causes off-fault plastic strain, which may either activate preexisting faults or initiate new faults. Fault development, however, is also controlled by the inherited lithospheric heterogeneities, which are poorly constrained and difficult to implement in model. Nonetheless, our results suggest that the initiation of young faults in Southern California in the past few million years are largely consequential to previous fault development. The Big Bend is shown to localize strain along the ECSZ and the Garlock Fault (Figures 3–5), thus may have contributed to the initiation of these fault zones, which initiated around the same time as the formation of the Big Bend. Similarly, the San Jacinto Fault and the younger subparallel faults to its west initiated in places of high plastic strain predicted by models that do not explicitly include these faults. These results can be conceptually understood as the plate boundary fault system constantly evolves to seek for the optimal pathways to accommodate the relative plate motion, as suggested by previous studies [*Cooke and Kameda*, 2002; *Liu et al*., 2010].

Although the predicted strain localization is illustrative for fault development, we did not try to explain the cause of each young fault because of the lack of constraints on the inherited lithospheric heterogeneities. Instead, we focused on the impact of each new fault on the regional partitioning of plastic strain and slip rates on the major faults. The changes of slip rates on segments of the SAF proper due to addition of each younger

fault in the model are summarized in Figure 10. The changes due to development of young secondary faults are significant, from 5 to 20 mm/yr. The absolute values of these changes depend on model parameters, especially the plastic strength assumed for each fault; but the general trend is physically robust. The southern segments of the southern SAF have the larger variation of slip rates compared to the northern segments, because of the initiation of numerous secondary faults in Southern California. Specifically, the initiation of the San Jacinto Fault, the Elsinore Fault, and the offshore faults in the past couple of million years reduced slip rates on the southernmost segments of SAF, while slip rates on the Mojave and Carrizo segments of the SAF increased because of increased dextral crustal motion on the western side of the plate boundary zone facilitated by these young faults.

The uncertainties of the initiation time of faults (Table 1) could affect the sequence of faults implemented in the models. For example, it is possible that the northern Elsinore Fault and some thrust faults in western Transverse Ranges may have initiated earlier than the San Jacinto Fault. However, these uncertainties do not change our main findings in those cases (Figures 7–9). Even if the northern Elsinore Fault was included in the model before the San Jacinto Fault, initiation of San Jacinto Fault would still reduce both plastic strain along the coastal region and slip rates on the southernmost segments of the SAF.

5.2. Codependence of Fault Slip Rates

Bennett et al. [2004], based on the estimated slip rate history for the past 5 Ma, proposed a codependence of the slip rate on the San Jacinto Fault and the southern SAF: the increase of slip rate on one fault decreases slip rate on the other. This apparent codependence of fault slip rates has been questioned by some recent studies. *Blisniuk et al*. [2013], for example, have shown that the observed slip on the San Jacinto Fault is stable during the last ~700 ka and argued that this is inconsistent with the model of codependent slip rates and its underlying physics—that slip rates are time dependent, and increase on one fault would cause decrease on the other fault. The uncertainties of the available estimates of slip rates have not permitted this issue to be fully resolved.

Our results may shed some light on this issue. When the San Jacinto Fault and the southern SAF are the only dextral faults in Southern California to accommodate the relative plate motion, then increasing slip rate on one fault would necessarily reduce slip rates on the other (Figure 7c). A more detailed discussion of the dynamic interactions between these two faults was given by *Luo and Liu* [2012]. The slip rate codependence between these two faults becomes more complicated when additional faults are involved in accommodating the relative plate motion. For example, initiation of the Elsinore Fault and the offshore faults would reduce slip rates on both the San Jacinto Fault and the southernmost SAF (Figure 8c). When more faults are involved, the slip distribution among them becomes more complicated. In reality, each of the faults modeled in our study consists of many fault strands and branches [*Zeng and Shen*, 2016], and many more faults are not included in the model. On the other hand, the initiation of the Elsinore and the offshore faults in the past one million years caused only <3 mm/yr change of slip rates on the San Jacinto Fault (Figures 8c and 9c); thus, an apparently stable slip rate on the San Jacinto Fault since 700 ka may not resolve changes of slip rates on other faults.

Our model results also suggest a more general slip rate codependence between the faults on the eastern and western sides of the broad plate boundary zone in Southern California. For example, increase of slip rates in the ECSZ tends to promote slip on the southernmost segments of the SAF (Figure 6c), which are aligned with the ECSZ on the eastern side of the plate boundary zone and are structurally connected [*Dokka and Travis*, 1990; *Thatcher et al*., 2016]. For similar reasons, initiation of the Elsinore and the offshore faults improves the mechanical efficiency of faults on the western side of the plate boundary zone, thus increasing slip rates on the Carrizo and the Big Bend segments of the SAF, which are aligned with these faults (Figure 8c). More geological measurements of slip rates are needed to test this hypothetical codependence of slip rate.

5.3. Discrepancy Between the Geological and Geodetic Slip Rates

Our results of fault evolution in Southern California and its impact on slip rates may help understand the slip rate discrepancy between geological and geodetic measurements (Figure 11). For example, the geodetic slip rate [*Becker et al*., 2005; *Meade and Hager*, 2005] along the San Bernardino segment of southern SAF are lower than geological estimates [*McGill et al*., 2013]; and the geodetic slip rate on the Mojave part of the ECSZ [*Loveless and Meade*, 2011] is almost two times the geological estimates [*Oskin et al*., 2008].

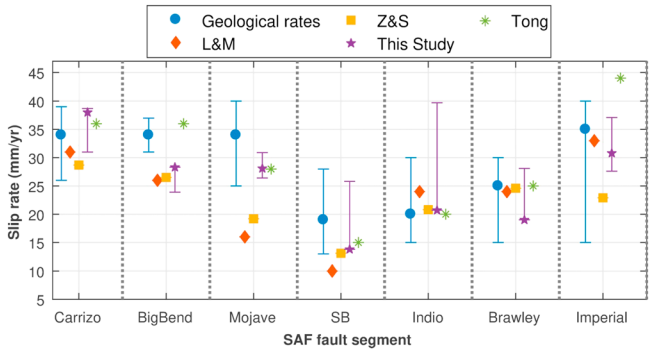

Figure 11. Comparison of the geological, geodetic, and our model-predicted slip rates on major SAF segments. The "Geological rates" are from USGS (Appendix B of the UCERF 3, http://pubs.usgs.gov/of/2013/1165/); "L&M" are the rates from geodetic inversion by *Loveless and Meade* [2011]; "'Z&S" are the rates from geodetic inversion by *Zeng and Shen* [2014]; "Tong" are the rates from geodetic inversion by *Tong et al.* [2014]; "This study" are the predicted slip rates with configuration of faults shown in Figure 10, and the ranges are given by the maximum and minimal value of slip rates in the cases shown in Figures 3–10.

Besides the intrinsic uncertainties in the geological estimates and geodetic inversion, different timescales are likely a major cause for these discrepancies. Geodetic data, collected over years to decades, are dominated by interseismic strain and are essentially snapshots of the present-day strain rates field, whereas geological slip rates are estimated from offsets that span over much longer time. Our results, based on simulation of steady state plastic creeping of fault zones and thus are comparable with geological slip rates, show that the evolution of the fault system in the plate boundary zone would impact slip rates on each individual fault. The slip rates on different segments of the SAF proper may have changed up to 20 mm/yr in the past 5 Ma (Figure 10). In the past one million years, the time span for most of the estimates of geological slip rates, the predicted slip rate on the southern segments of the SAF may have changed as much as 10 mm/yr (Figure 10). Although these values need to be taken with caution because of their dependence on the assumed fault strength, the general trends of the predicted changes are consistent with the observed slip rate discrepancy. For example, a decrease of slip rates on the SAF-San Bernardino segment is predicted after the initiation of the Elsinore and the offshore dextral faults (Figure 8c), which reduce the relative plate motion that need to be accommodated by the southern SAF. This decrease of slip rate on the SAF-San Bernardino segment is consistent with geological data, which show higher rate (28 mm/yr) by averaging the total bedrock offset of 140 km along the San Bernardino section over the past 5 Ma [*Matti and Morton*, 1993] and lower rate (6.8–16.3 mm/yr) over the past 35 ka based on the offset history [*McGill et al.*, 2013]. This recent slip rate is closer to the geodetic estimation of present-day rate [*Loveless and Meade*, 2011; *Tong et al.*, 2014; *Zeng and Shen*, 2014] (Figure 11).

Given the complexity of fault systems in nature, selecting the faults and fault strands for evaluation is a challenge for both geological and geodetic estimates of slip rates. Recent studies reevaluating the kinematic models of inverting geodetic slip rate suggest that around 20–40% of the total strain across the ECSZ may be accommodated by the off-fault deformation [*Johnson*, 2013; *Herbert et al.*, 2014]. We face the same challenge in our geodynamic model. The faults we implemented in the model are first-order approximations; they serve the purpose of illustrating the general impact of these faults on the regional strain partitioning and slip rates on the major faults. On the other hand, by calculating plastic strain that would localize in the off-fault crust, our results provide some insights on the causes of young faults and the general evolution of the plate boundary fault system.

6. Conclusions

We have used a three-dimensional viscoelastic-plastic geodynamic model to investigate how fault evolution in the Southern California plate boundary zone may have changed regional strain partitioning and fault slip rates in the past few million years. The major conclusions we may draw include the following:

1. The formation of the restraining Big Bend has had a dominant influence on the subsequent development of the plate boundary zone in Southern California. The Big Bend impedes relative plate motion on the San Andreas proper and forces off-fault plastic strain. The Eastern California Shear Zone (ECSZ), the Garlark Fault, the San Jacinto Fault, the Elsinore Fault, and the offshore faults all developed in places of predicted high plastic strain rates, suggesting that the initiation of these younger faults are largely

influenced by the evolving fault configuration, as the plate boundary zone continues to seek for the optimal paths to accommodate the relative plate motion.

2. Initiation of the San Jacinto Fault in the past ~2 Ma has significantly reduced slip rate on the subparallel segments of the southern SAF. Initiation of the Elsinore and the offshore dextral faults in the past one million years has reduced slip rates on both the San Jacinto Fault and the southernmost SAF, and localized strain in the western Transverse Ranges.
3. Our results support the hypothesis of codependent slip rate between the San Jacinto Fault and southern SAF, although this codependence is weakened in the past one million years by the initiation of numerous younger subparallel dextral faults. Furthermore, our results suggest a general codependence of slip rates among all the NW trending dextral faults in the Southern California plate boundary zone, because they collectively accommodate the relative plate motion between the Pacific and the North American plates. Slip on the ECSZ promotes slip on the southernmost segments of the southern SAF, which are aligned and structurally linked with the ECSZ. Conversely, slip on the Elsinore and the offshore dextral faults increases slip on the SAF segments on the western sides of the Southern California plate boundary zone.
4. The initiation of numerous young faults in the past couple of million years may have contributed to the observed discrepancy between geological and geodetic estimates of fault slip rates in Southern California.
5. Our model with the present fault configuration predicts high strain rates in western Transverse Ranges and the ECSZ across the Mojave Desert, where fault slip rates are not well constrained but numerous damaging earthquakes occurred in recent years.

Acknowledgments
This work was supported by NSF grant EAR-0948620. We thank Hui Wang for assisting in the computation and Huai Zhang for help with the computer code development. We thank Editor Uri ten Brink of JGR for handling the paper and one Associate Editor and one anonymous reviewer for their constructive reviews. The finite element code used in this study was developed by *Li et al*. [2009], which may be requested by contacting one of the coauthors at: lium@missouri.edu.

References

Albright, L. B. (1999), Magnetostratigraphy and biochronology of the San Timoteo Badlands, Southern California, with implications for local Pliocene–Pleistocene tectonic and depositional patterns, *Geol. Soc. Am. Bull.*, *111*(9), 1265–1293.

Atwater, T. (1970), Implications of plate tectonics for the Cenozoic tectonic evolution of western North America, *Geol. Soc. Am. Bull.*, *81*(12), 3513–3536.

Atwater, T., and J. Stock (1998), Pacific-North America plate tectonics of the Neogene southwestern United States: An update, *Int. Geol. Rev.*, *40*, 375–402.

Becker, T. W., J. L. Hardebeck, and G. Anderson (2005), Constraints on fault slip rates of the Southern California plate boundary from GPS velocity and stress inversions, *Geophys. J. Int.*, *160*, 634–650, doi:10.1111/j.1365-246X.2004.02528.x.

Bellier, O., and M. L. Zoback (1995), Recent state of stress change in the Walker Lane zone, western Basin and Range province, United States, *Tectonics*, *14*(3), 564–593.

Bennett, R. A., W. Rodi, and R. E. Reilinger (1996), Global Positioning System constraints on fault slip rates in southern California and northern Baja, Mexico, *J. Geophys. Res.*, *101*(B10), 21943–21960.

Bennett, R. A., A. M. Friedrich, and K. P. Furlong (2004), Codependent histories of the San Andreas and San Jacinto fault zones from inversion of fault displacement rates, *Geology*, *32*(11), 961–964, doi:10.1130/g20806.1.

Bird, P. (2007), Uncertainties in long-term geologic offset rates of faults: General principles illustrated with data from California and other western states, *Geosphere*, *3*(6), 577–595, doi:10.1130/GES00127.1.

Bird, P. (2009), Long-term fault slip rates, distributed deformation rates, and forecast of seismicity in the western United States from joint fitting of community geologic, geodetic, and stress direction data sets, *J. Geophys. Res.*, *114*, B11403, doi:10.1029/2009JB006317.

Bird, P., and X. Kong (1994), Computer simulations of California tectonics confirm very low strength of major faults, *Geol. Soc. Am. Bull.*, *106*(2), 159–174.

Blisniuk, K., M. Oskin, A.-S. Mériaux, T. Rockwell, R. C. Finkel, and F. J. Ryerson (2013), Stable, rapid rate of slip since inception of the San Jacinto fault, California, *Geophys. Res. Lett.*, *40*, 4209–4213, doi:10.1002/grl.50819.

Bourne, S. J., P. C. England, and B. Parsons (1998), The motion of crustal blocks driven by flow of the lower lithosphere and implications for slip rates of continental strike-slip faults, *Nature*, *391*, 655–659.

Burbank, D. W., and D. P. Whistler (1987), Temporally constrained tectonic rotations derived from magnetostratigraphic data: Implications for the initiation of the Garlock fault, California, *Geology*, *15*(12), 1172–1175.

Chuang, R. Y., and K. M. Johnson (2011), Reconciling geologic and geodetic model fault slip-rate discrepancies in Southern California: Consideration of nonsteady mantle flow and lower crustal fault creep, *Geology*, *39*(7), 627–630, doi:10.1130/G32120.1.

Cook, R. D., D. S. Malkus, M. E. Plesha, and R. J. Witt (2002), *Concepts and Applications of Finite Element Analysis*, John Wiley, New York.

Cooke, M. L., and L. C. Dair (2011), Simulating the recent evolution of the southern big bend of the San Andreas fault, Southern California, *J. Geophys. Res.*, *116*, B04405, doi:10.1029/2010JB007835.

Cooke, M. L., and A. Kameda (2002), Mechanical fault interaction within the Los Angeles Basin: A two-dimensional analysis using mechanical efficiency, *J. Geophys. Res.*, *107*(B7), ETG 10-1–ETG 10-15, doi:10.1029/2001JB000542.

Davis, G. A., and B. Burchfiel (1973), Garlock fault: An intracontinental transform structure, Southern California, *Geol. Soc. Am. Bull.*, *84*(4), 1407–1422.

DeMets, C., R. G. Gordon, D. F. Argus, and S. Stein (1994), Effect of recent revisions to the geomagnetic reversal time scale on estimates of current plate motions, *Geophys. Res. Lett.*, *21*(20), 2191–2194.

Dixon, T. H., M. Miller, F. Farina, H. Wang, and D. Johnson (2000), Present-day motion of the Sierra Nevada block and some tectonic implications for the Basin and Range province, North American Cordillera, *Tectonics*, *19*(1), 1–24.

Dixon, T. H., E. Norabuena, and L. Hotaling (2003), Paleoseismology and Global Positioning System: Earthquake-cycle effects and geodetic versus geologic fault slip rates in the eastern California shear zone, *Geology*, *31*(1), 55–58.

Dokka, R. K., and C. J. Travis (1990), Role of the eastern California shear zone in accommodating Pacific-North American plate motion, *Geophys. Res. Lett.*, *17*(9), 1323–1326.

Dolan, J. F., K. Sieh, T. K. Rockwell, R. S. Yeats, J. Shaw, J. Suppe, G. J. Huftile, and E. M. Gath (1995), Prospects for larger or more frequent earthquakes in the Los Angeles metropolitan region, *Science*, *267*(5195), 199–205, doi:10.1126/science.267.5195.199.

Dorsey, R. J. (2002), Stratigraphic record of Pleistocene initiation and slip on the Coyote Creek fault, lower Coyote Creek, southern California, *Geol. Soc. Am. Spec. Pap.*, *365*, 251–270.

Dorsey, R. J., G. J. Axen, T. C. Peryam, and M. E. Kairouz (2012), Initiation of the Southern Elsinore Fault at ~1.2 Ma: Evidence from the Fish Creek–Vallecito Basin, Southern California, *Tectonics*, *31*, TC2006, doi:10.1029/2011TC003009.

Drucker, D. C., and W. Prager (1952), Soil mechanics and plastic analysis or limit design, *Quart. Appl. Math.*, *10*, 157–165.

England, P., and P. Molnar (1997), Active deformation of Asia: From kinematics to dynamics, *Science*, *278*(5338), 647.

Evans, E. L., W. R. Thatcher, F. F. Pollitz, and J. R. Murray (2016), Persistent slip rate discrepancies in the eastern California (USA) shear zone, *Geology*, *44*(9), 691–694, doi:10.1130/G37967.1.

Flesch, L. M., W. E. Holt, A. J. Haines, and B. Shen-Tu (2000), Dynamics of the Pacific-North American plate boundary in the western United States, *Science*, *287*(5454), 834–836.

Gan, W., J. Svarc, J. Savage, and W. Prescott (2000), Strain accumulation across the eastern California shear zone at latitude 36°30′N, *J. Geophys. Res.*, *105*(B7), 16229–16236.

Ganev, P. N., J. F. Dolan, S. F. McGill, and K. L. Frankel (2012), Constancy of geologic slip rate along the central Garlock fault: Implications for strain accumulation and release in southern California, *Geophys. J. Int.*, *190*(2), 745–760, doi:10.1111/j.1365-246X.2012.05494.x.

Grant, L. B., and P. M. Shearer (2004), Activity of the offshore Newport-Inglewood rose canyon fault zone, coastal Southern California, from relocated microseismicity, *Bull. Seismol. Soc. Am.*, *94*(2), 747–752.

Grant, L. B., J. T. Waggoner, T. K. Rockwell, and C. von Stein (1997), Paleoseismicity of the north branch of the Newport-Inglewood fault zone in Huntington Beach, California, from cone penetrometer test data, *Bull. Seismol. Soc. Am.*, *87*(2), 277–293.

Herbert, J. W., M. L. Cooke, M. Oskin, and O. Difo (2014), How much can off-fault deformation contribute to the slip rate discrepancy within the eastern California shear zone?, *Geology*, *42*(1), 71–75, doi:10.1130/g34738.1.

Hill, M. L. (1971), Newport-Inglewood zone and Mesozoic subduction, California, *Geol. Soc. Am. Bull.*, *82*(10), 2957–2962.

Hill, M. L., and T. W. Dibblee (1953), San Andreas, Garlock, and Big Pine Faults, California, *Geol. Soc. Am. Bull.*, *64*(4), 443, doi:10.1130/0016-7606(1953)64[443:sagabp]2.0.co;2.

Holt, J. W., E. W. Holt, and J. M. Stock (2000), An age constraint on Gulf of California rifting from the Santa Rosalía basin, Baja California Sur, Mexico, *Geol. Soc. Am. Bull.*, *112*(4), 540–549.

Huftile, G. J., and R. S. Yeats (1995), Convergence rates across a displacement transfer zone in the western transverse ranges, Ventura basin, California, *J. Geophys. Res.*, *100*(B2), 2043–2067.

Hull, A. G., and G. Nicholson (1992), Seismotectonics of the northern Elsinore fault zone, southern California, *Bull. Seismol. Soc. Am.*, *82*, 800–818.

Janecke, S. U., R. J. Dorsey, D. Forand, A. N. Steely, S. M. Kirby, A. T. Lutz, B. A. Housen, B. Belgarde, V. E. Langenheim, and T. M. Rittenour (2011), High geologic slip rates since Early Pleistocene initiation of the San Jacinto and San Felipe fault zones in the San Andreas fault system: Southern California, USA, *Geol. Soc. Am. Spec. Pap.*, *475*, 1–48.

Johnson, K. (2013), Slip rates and off-fault deformation in Southern California inferred from GPS data and models, *J. Geophys. Res. Solid Earth*, *118*, 5643–5664, doi:10.1002/jgrb.50365.

Kirby, E., D. W. Burbank, M. Reheis, and F. Phillips (2006), Temporal variations in slip rate of the White Mountain fault zone, eastern California, *Earth Planet. Sci. Lett.*, *248*, 168–185, doi:10.1016/j.epsl.2006.05.026.

Li, Q., and M. Liu (2006), Geometrical impact of the San Andreas fault on stress and seismicity in California, *Geophys. Res. Lett.*, *33*, L08302, doi:10.1029/2005GL025661.

Li, Q., and M. Liu (2007), Initiation of the San Jacinto fault and its interaction with the San Andreas fault: Insights from geodynamic modeling, *Pure Appl. Geophys.*, *164*, 1937–1945, doi:10.1007/s00024-007-0262-z.

Li, Q., M. Liu, and H. Zhang (2009), A 3-D viscoelastoplastic model for simulating long-term slip on non-planar faults, *Geophys. J. Int.*, *176*(1), 293–306.

Lindsey, E. O., and Y. Fialko (2013), Geodetic slip rates in the southern San Andreas fault system: Effects of elastic heterogeneity and fault geometry, *J. Geophys. Res. Solid Earth*, *118*, 689–697, doi:10.1029/2012JB009358.

Liu, M., H. Wang, and Q. Li (2010), Inception of the eastern California shear zone and evolution of the Pacific-north American plate boundary: From kinematics to geodynamics, *J. Geophys. Res.*, *115*, B07401, doi:10.1029/2009JB007055.

Loveless, J. P., and B. J. Meade (2011), Stress modulation on the San Andreas fault by interseismic fault system interactions, *Geology*, *39*, 1035–1038 ST- Stress modulation on the San Andre, doi:10.1130/g32215.1.

Lundgren, P., E. A. Hetland, Z. Liu, and E. J. Fielding (2009), Southern San Andreas-San Jacinto fault system slip rates estimated from earthquake cycle models constrained by GPS and interferometric synthetic aperture radar observations, *J. Geophys. Res.*, *114*, B02403, doi:10.1029/2008JB005996.

Luo, G., and M. Liu (2012), Multi-timescale mechanical coupling between the San Jacinto fault and the San Andreas fault, southern California, *Lithosphere*, *4*, 221–229, doi:10.1130/L180.1131.

Lutz, A. T., R. J. Dorsey, B. A. Housen, and S. U. Janecke (2006), Stratigraphic record of Pleistocene faulting and basin evolution in the Borrego Badlands, San Jacinto fault zone, Southern California, *Geol. Soc. Am. Bull.*, *118*(11–12), 1377–1397.

Magistrale, H., and T. Rockwell (1996), The central and southern Elsinore fault zone, southern California, *Bull. Seismol. Soc. Am.*, *86*, 1793–1803.

Matti, J. C., and D. M. Morton (1993), Chapter 2: Paleogeographic evolution of the San Andreas fault in southern California: A reconstruction based on a new cross-fault correlation, *Geol. Soc. Am. Mem.*, *178*, 107–160, doi:10.1130/MEM178-p107.

McCaffrey, R. (2005), Block kinematics of the Pacific–North America plate boundary in the southwestern United States from inversion of GPS, seismological, and geologic data, *J. Geophys. Res.*, *110*, B07401, doi:10.1029/2004JB003307.

McGill, S. F., S. G. Wells, S. K. Fortner, H. A. Kuzma, and J. D. McGill (2009), Slip rate of the western Garlock fault, at Clark Wash, near Lone Tree Canyon, Mojave Desert, California, *Geol. Soc. Am. Bull.*, *121*(3–4), 536–554, doi:10.1130/b26123.1.

McGill, S. F., L. A. Owen, R. J. Weldon, and K. J. Kendrick (2013), Latest Pleistocene and Holocene slip rate for the San Bernardino strand of the San Andreas fault, Plunge Creek, Southern California: Implications for strain partitioning within the southern San Andreas fault system for the last ~35 k.Y, *Geol. Soc. Am. Bull.*, *125*(1–2), 48–72, doi:10.1130/b30647.1.

McGill, S. F., J. C. Spinler, J. D. McGill, R. A. Bennett, M. A. Floyd, J. E. Fryxell, and G. J. Funning (2015), Kinematic modeling of fault slip rates using new geodetic velocities from a transect across the Pacific-North America plate boundary through the San Bernardino Mountains, California, *J. Geophys. Res. Solid Earth*, *120*, 2772–2793, doi:10.1002/2014JB011459.

McNeilan, T. W., T. K. Rockwell, and G. S. Resnick (1996), Style and rate of Holocene slip, Palos Verdes fault, southern California, *J. Geophys. Res.*, *101*(B4), 8317–8334.

Meade, B. J., and B. H. Hager (2005), Block models of crustal motion in southern California constrained by GPS measurements, *J. Geophys. Res.*, *110*, B03403, doi:10.1029/2004JB003209.
Monastero, F., A. Sabin, and J. Walker (1997), Evidence for post-early Miocene initiation of movement on the Garlock fault from offset of the Cudahy Camp Formation, east-central California, *Geology*, *25*(3), 247–250.
Morton, D. M., and J. C. Matti (1993), Extension and contraction within an evolving divergent strike-slip fault complex: The San Andreas and San Jacinto fault zones at their convergence in Southern California, in *The San Andreas Fault System: Displacement, Palinspastic Reconstruction, and Geologic Evolution*, edited by R. E. Powell, R. J. Weldon, and J. C. Matti, pp. 217–230, Geol. Soc. Am. Mem., Boulder, Colo.
Namson, J., and T. Davis (1988), Structural transect of the western transverse ranges, California: Implications for lithospheric kinematics and seismic risk evaluation, *Geology*, *16*(8), 675–679.
Oskin, M., and J. Stock (2003), Pacific–North America plate motion and opening of the upper Delfín basin, northern Gulf of California, Mexico, *Geol. Soc. Am. Bull.*, *115*, 1173–1190, doi:10.1130/B25154.1.
Oskin, M., L. Perg, E. Shelef, M. Strane, E. Gurney, B. Singer, and X. Zhang (2008), Elevated shear zone loading rate during an earthquake cluster in eastern California, *Geology*, *36*(6), 507–510, doi:10.1130/G24814A.1.
Peltzer, G., F. Crampé, S. Hensley, and P. Rosen (2001), Transient strain accumulation and fault interaction in the eastern California shear zone, *Geology*, *29*, 975.
Rockwell, T., C. Loughman, and P. Merifield (1990), Late Quaternary rate of slip along the San Jacinto fault zone near Anza, southern California, *J. Geophys. Res.*, *95*(B6), 8593–8605.
Sharp, R. V. (1981), Variable rates of late Quaternary strike slip on the San Jacinto fault zone, southern California, *J. Geophys. Res.*, *86*(B3), 1754–1762.
Spinler, J. C., R. A. Bennett, M. L. Anderson, S. F. McGill, S. Hreinsdóttir, and A. McCallister (2010), Present-day strain accumulation and slip rates associated with southern San Andreas and eastern California shear zone faults, *J. Geophys. Res.*, *115*, B11407, doi:10.1029/2010JB007424.
Stock, J., and K. Hodges (1989), Pre-Pliocene extension around the Gulf of California and the transfer of Baja California to the Pacific Plate, *Tectonics*, *8*(1), 99–115.
Thatcher, W., J. C. Savage, and R. W. Simpson (2016), The eastern California shear zone as the northward extension of the southern San Andreas Fault, *J. Geophys. Res. Solid Earth*, *121*, 2904–2914, doi:10.1002/2015JB012678.
Tong, X., B. Smith-Konter, and D. T. Sandwell (2014), Is there a discrepancy between geological and geodetic slip rates along the San Andreas fault system?, *J. Geophys. Res. Solid Earth*, *119*, 2518–2538, doi:10.1002/2013JB010765.
Townend, J., and M. Zoback (2004), Regional tectonic stress near the San Andreas fault in central and southern California, *Geophys. Res. Lett.*, *31*, L15S11, doi:10.1029/2003GL018918.
Wallace, R. E. (1990), The San Andreas fault system, California, *U.S. Geol. Surv. Prof. Pap., 1515*.
Ward, S. N., and G. Valensise (1994), The Palos Verdes terraces, California: Bathtub rings from a buried reverse fault, *J. Geophys. Res.*, *99*(B3), 4485–4494.
Wernicke, B., and J. K. Snow (1998), Cenozoic tectonism in the central Basin and Range: Motion of the Sierran-Great Valley block, *Int. Geol. Rev.*, *40*(5), 403–410.
Ye, J., M. Liu, and H. Wang (2015), A numerical study of strike-slip bend formation with application to the Salton Sea pull-apart basin, *Geophys. Res. Lett.*, *42*, 1368–1374, doi:10.1002/2015GL063180.
Zechar, J. D., and L. F. Kurt (2009), Incorporating and reporting uncertainties in fault slip rates, *J. Geophys. Res.*, *114*, B12407, doi:10.1029/2009JB006325.
Zeng, Y., and Z.-K. Shen (2014), Fault network modeling of crustal deformation in California constrained using GPS and geologic observations, *Tectonophysics*, *612–613*, 1–17, doi:10.1016/j.tecto.2013.11.030.
Zeng, Y., and Z. K. Shen (2016), A fault-based model for crustal deformation, fault slip rates, and off-fault strain rate in California, *Bull. Seismol. Soc. Am.*, *106*(2), 766–784, doi:10.1785/0120140250.
Zoback, M. L., R. Anderson, and G. Thompson (1981), Cainozoic evolution of the state of stress and style of tectonism of the Basin and Range province of the western United States, *Philos. Trans. R. Soc. Lond. A*, *300*(1454), 407–434.